Donnelly et al., https://doi.org/10.1083/jcb.201704048

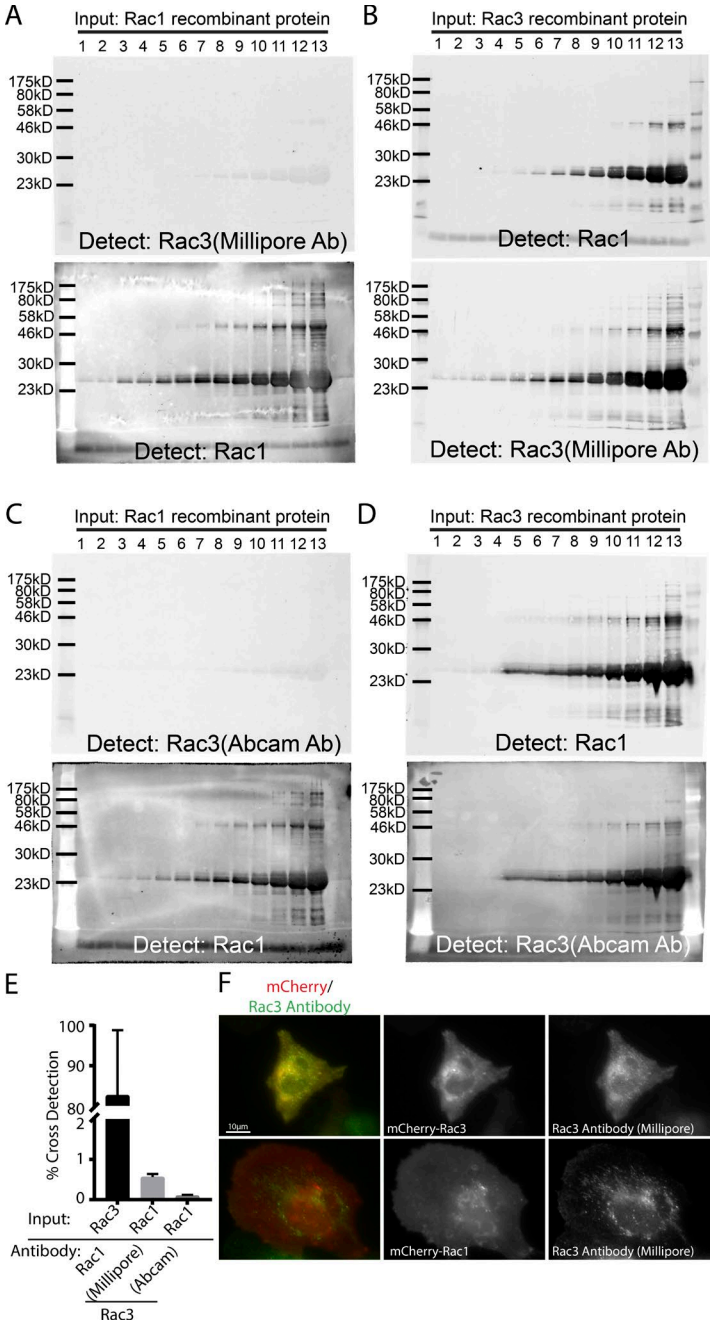

Figure S1. **Specificity of Rac3 antibody.** (A–D) Purified Rac1 and Rac3 proteins were loaded in increasing amounts per well (lanes 1–13) and detected using indicated antibodies. (A and C) Purified Rac1 was added to lanes in the following amounts: lane 1, 4.4 ng; lane 2, 8.8 ng; lane 3, 17.5 ng; lane 4, 35.1 ng; lane 5, 70.1 ng; lane 6, 140.3 ng; lane 7, 280.5 ng; lane 8, 561.1 ng; lane 9, 1.1 µg; lane 10, 2.2 µg; lane 11, 4.5 µg; lane 12, 9.0 µg; and lane 13, 18.0 µg. (B and D) Purified Rac3 protein was added to lanes in the following amounts: lane 1, 4.5 ng; lane 2, 9.1 ng; lane 3, 18.1 ng; lane 4, 36.3 ng; lane 5, 72.6 ng; lane 6, 145.2 ng; lane 7, 290.4 ng; lane 8, 580.8 ng; lane 9, 1.2 µg; lane 10, 2.3 µg; lane 11, 4.6 µg; lane 12, 9.3 µg; and lane 13, 18.6 µg. Purification of Rac1 and Rac3 proteins were performed following well-established protocols (Smith and Rittinger, 2002). The top blots of A and B as well as C and D, were detected simultaneously together in the Odyssey imager under the same gain setting to maintain relative intensities of signals from the CW800 dye–conjugated secondary antibodies used in detection. In the bottom blots in A and B as well as C and D, they were detected together simultaneously in the Odyssey imager under the same gain settings using LT-670–conjugated secondary antibodies. (E) Quantification of the percent cross-detection of the Rac1-specific antibody and the two Rac3-specific antibodies used in A–D. (F) MDA–MB-231 cells transfected with mCherry-Rac1 or mCherry-Rac3, plated on fibronectin, fixed, and stained with the EMD Millipore Rac3 antibody. The localization patterns of Rac1 detected by mCherry fluorescence appear different from that of Rac3 detected by antibody staining.

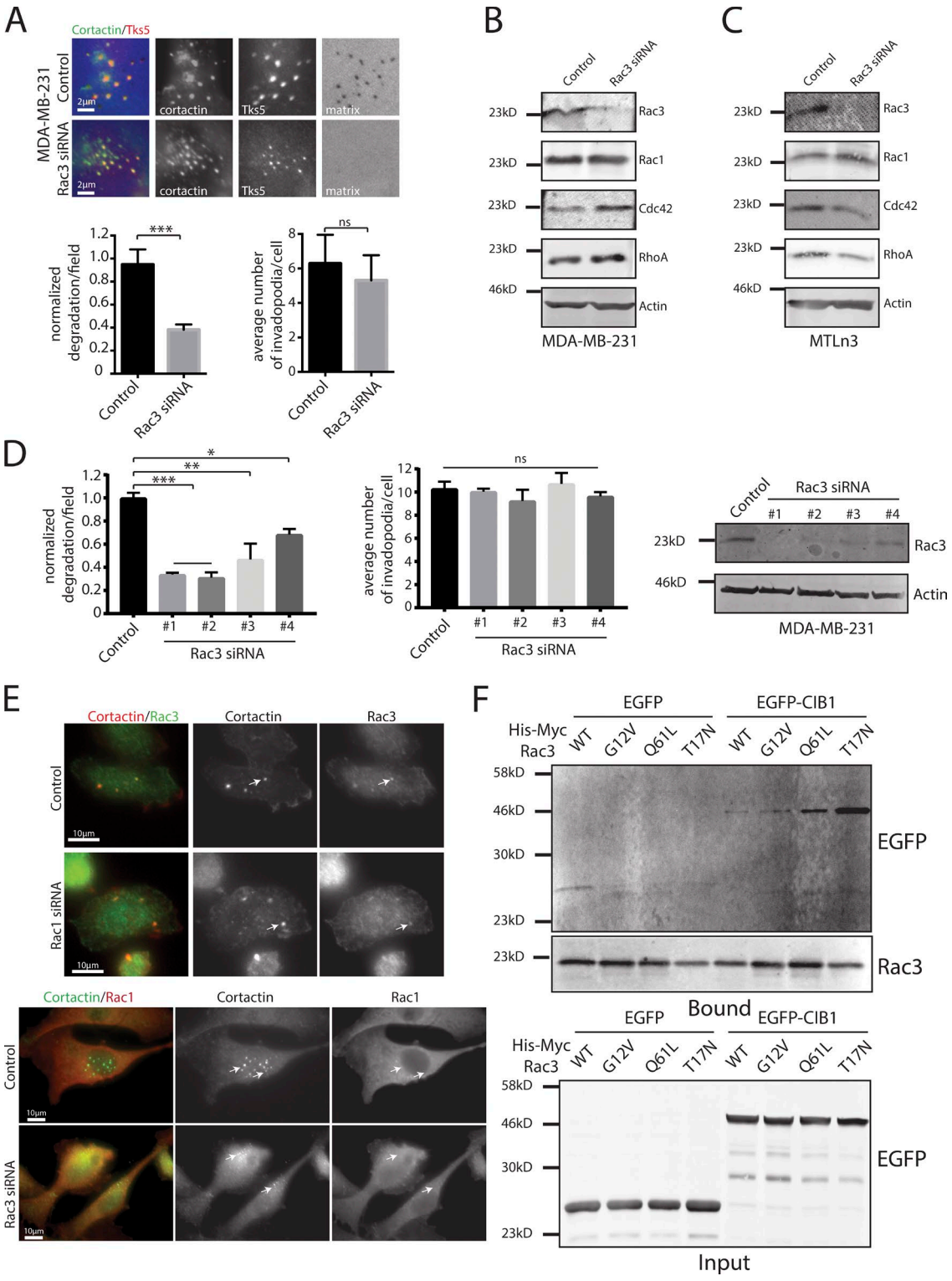

Figure S2. **Rac3 is enriched at invadopodia and required for matrix degradation.** (A) MDA–MB-231 cells transfected with control (top images) or Rac3 siRNA (bottom images) and plated on 405 nm fluorescent gelatin for 4 h. (A, bottom left) Normalized quantification of mean degradation area per field. $n \geq 10$ fields for each condition; three independent experiments. (A, bottom right) Quantification of the mean number of invadopodia per cell. $n \geq 50$ invadopodia from ≥20 cells for each condition for each of three independent experiments. (B) Western blot of cell lysates of control and Rac3 siRNA–treated MDA–MB-231 cells blotted for Rac3, Rac1, Cdc42, RhoA, and β-actin. (C) Western blot of cell lysates of control and Rac3 siRNA–treated MTLn3 cells blotted for Rac3, Rac1, Cdc42, RhoA, and β-actin. (D) Four single siRNAs from the siRNA Smartpool for Rac3 (rat) were individually tested for depletion and matrix degradation in MTLn3 cells. (E, top) Silencing of Rac1 did not alter the localization of Rac3 in MTLn3 cells. Representative Rac3 localization patterns are shown in control or Rac1-depleted MTLn3 cells. (E, bottom) Silencing of Rac3 did not alter the localization of Rac1 in MDA–MB-231 cells. Representative Rac1 localization patterns are shown in control or Rac3-depleted MDA–MB-231 cells. White arrows indicate invadopodia. (F) Western Blots of bound (top) or input (bottom) fraction of pulldowns from HEK293T cells coexpressing the indicated His-myc-Rac3 constructs (WT, constitutively active [G12V/Q61L], or DN [T17N]), with EGFP alone or EGFP-CIB1. *, $P \leq 0.05$; **, $P \leq 0.01$; ***, $P \leq 0.001$. All error bars are SEM.

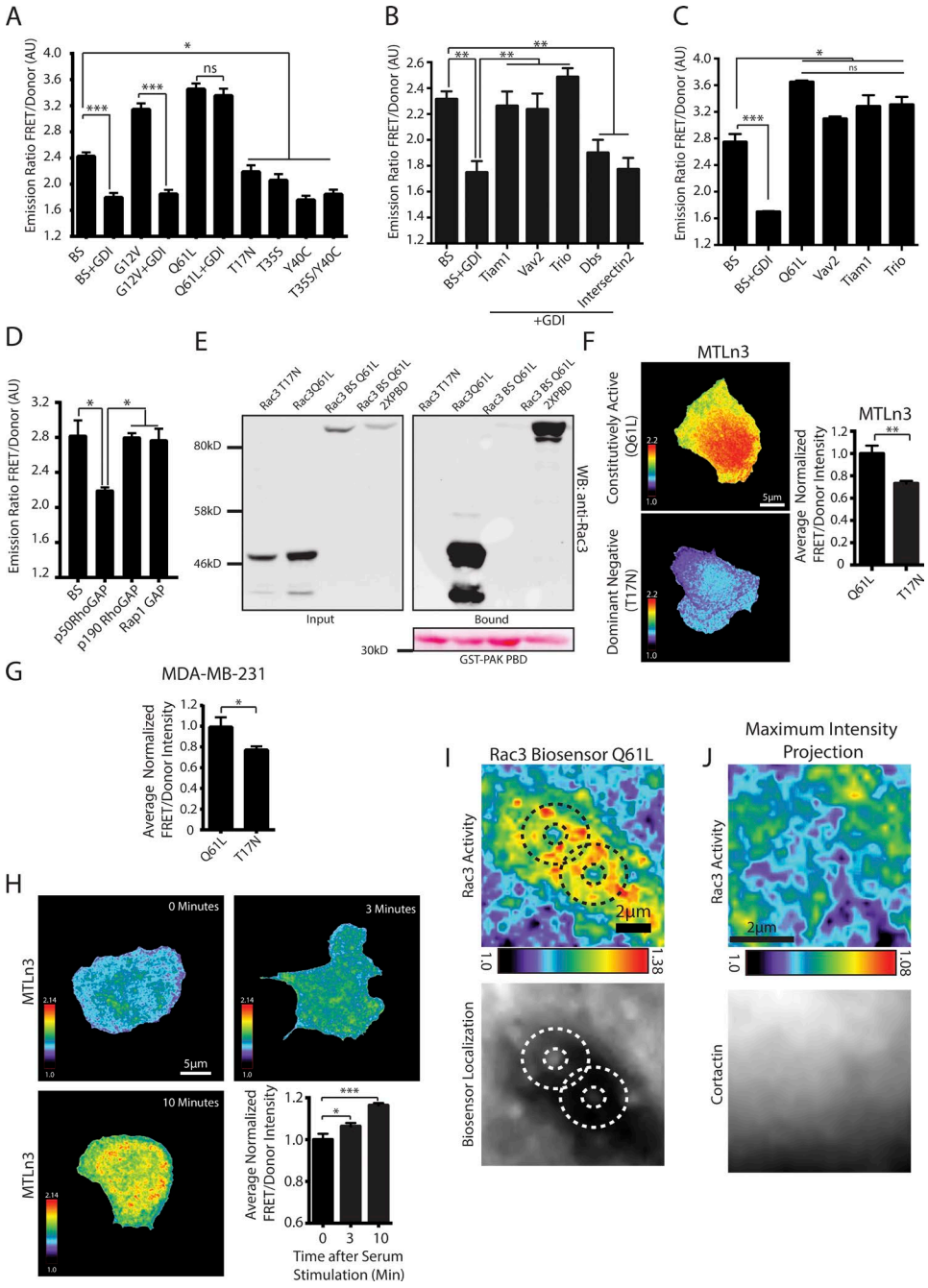

Figure S3. **A Rac3 FRET biosensor reveals two spatially distinct pools of Rac3 activity at invadopodia.** (A) Normalized emission ratios (FRET/donor) of WT biosensor (BS) and mutant (G12V, constitutively active Q61L, DN T17N, T35S, and effector binding–deficient Y40C) versions of the Rac3 biosensor coexpressed with or without excess (2×) GDI. The G12V mutant interacts with GDI, whereas the Q61L mutant does not. Ratios were calculated from emission spectra of biosensor mutants expressed in HEK293T cells (excitation at 433 nm; mCerulean1 was measured at 474 nm, and FRET was measured at 528 nm). (B) Normalized emission ratios (FRET/donor) of WT Rac3 biosensor coexpressed with GEF activators. Tiam1, Vav2, and Trio are Rac GEFs, and they rescue WT biosensor activity in the presence of excess (2×) GDI. Dbs and Intersectin2 do not have Rac GEF activity and are unable to rescue activity. (C) Normalized emission ratios (FRET/donor) of WT Rac3 biosensor coexpressed with GEF activators. In the absence of GDI, expression of the Rac-targeting GEFs Vav2, Tiam1, and Trio increase WT biosensor activity to near constitutively active (Q61L) levels. $n = 5$ independent experiments. (D) p50RhoGAP has GAP activity toward Rac and significantly reduces WT Rac3 biosensor FRET. P190RhoGAP and Rap1GAP do not have Rac GAP activity and have no effect on biosensor FRET. $n = 3$ independent experiments. (E) Pulldown demonstrating that the Rac3 biosensor only interacts with exogenous purified GST-PAK PBD if its own PBD domains are both mutated and unable to bind to Rac3 (2XPBD). Rac3-T17N and Rac3-Q61L are used as positive and negative controls, respectively. Ponceau S stain shows equal levels of PAK-PBD in each sample. (F) Representative images and quantification of FRET/donor intensity in MTLn3 cells expressing either constitutively active (Q61L) or DN (T17N) Rac3 biosensor. $n \geq 10$ cells for each condition. (G) Quantification of FRET/donor intensity in MDA–MB-231 cells expressing either constitutively active (Q61L) or DN (T17N) Rac3 biosensor. $n \geq 10$ cells for each condition. (H) Representative images and quantification of FRET/donor intensity in Rac3 biosensor expressing MTLn3 cells starved and stimulated with serum for the indicated times. $n \geq 10$ cells for each condition. (I) Images of Q61L, a constitutively active Rac3 biosensor, expressed in MDA–MB-231 cells, showing invadopodia-associated accumulation of Rac3 activity. Dashed lines highlight prominent rings of Rac3 activity surrounding points of accumulation of Rac3 biosensor (mCerulean1). (J) A representative maximum-intensity projection in time of Rac3 activity at a cellular region unrelated to invadopodia, shown as a negative control. *, $P \leq 0.05$; **, $P \leq 0.01$; ***, $P \leq 0.001$. All error bars are SEM. WB, Western blot.

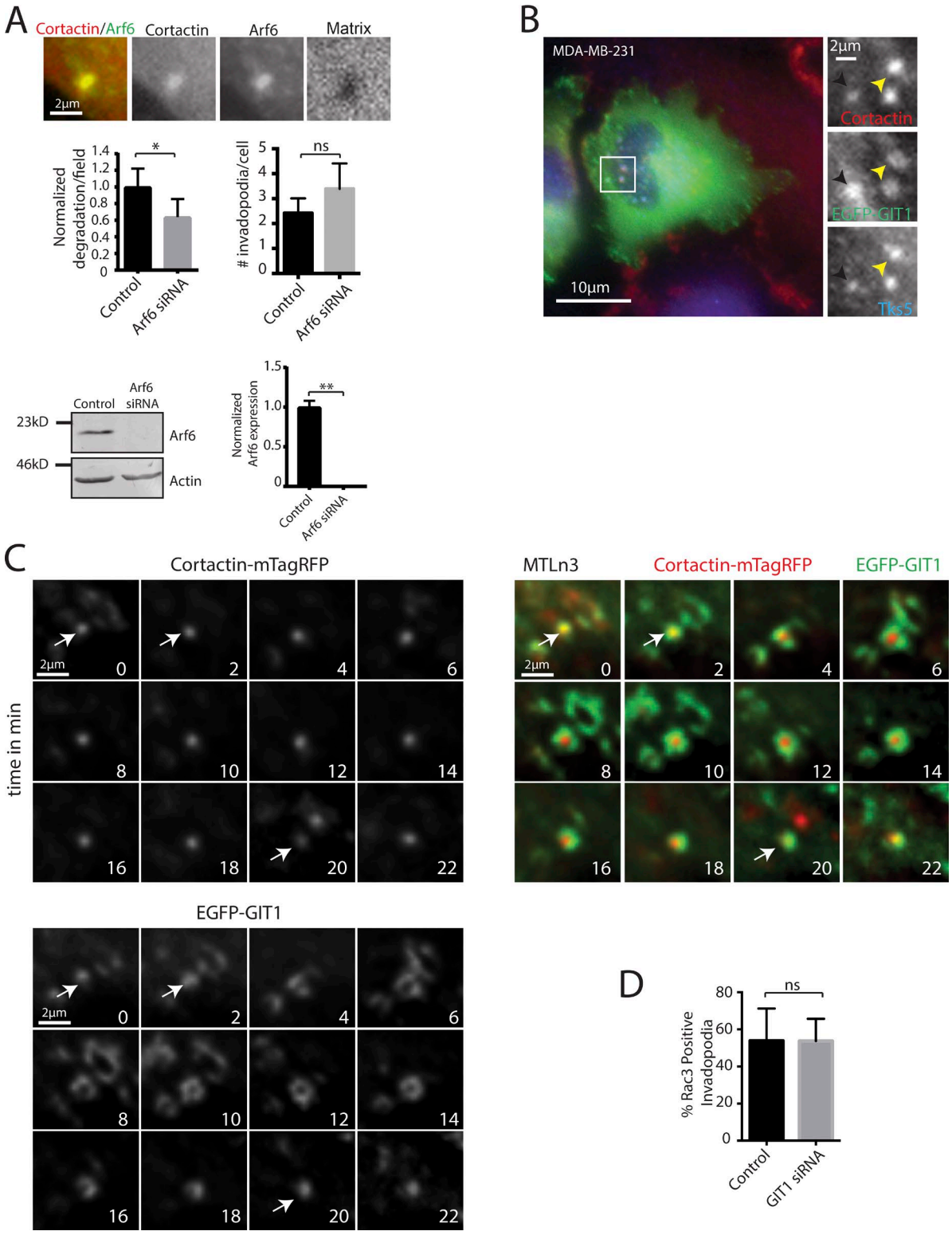

Figure S4. **Rac3 targets GIT1 to regulate MT1-MMP–mediated matrix degradation at invadopodia.** (A) Immunofluorescence image of endogenous Arf6 localized to an invadopod (identified by cortactin stain/matrix degradation) in an MTLn3 cell plated on 405 nm fluorescent gelatin for 16 h. (A, top left graph) Normalized quantification of mean degradation area per field. $n \geq 10$ fields for each condition for each of three independent experiments. (A, top right graph) Quantification of the mean number of invadopodia per cell. $n \geq 50$ invadopodia from ≥25 cells for each condition for three independent experiments. Western blot of cell lysates of control and Arf6 siRNA–treated MTLn3 cells blotted for Arf6 and β-actin with quantification. (B) Image of MDA–MB-231 cells expressing EGFP-GIT1. Yellow arrowheads point to ring localization of GIT1 at invadopodia (denoted by cortactin/Tks5), and black arrowheads point to core localization. (C) Montage of frames taken from a time-lapse video of MTLn3 cells showing the oscillation of EGFP-GIT1 at invadopodia denoted by cortactin-mTagRFP. Widefield microscopy was used to obtain these images, followed by image deconvolution. White arrows point to localization of EGFP-GIT1 at the core of invadopodia, denoted by cortactin. (D) Quantification of the percentage of Rac3-positive invadopodia in MTLn3 cells transfected with control or GIT1 siRNA. *, $P \leq 0.05$; **, $P \leq 0.01$. All error bars are SEM.

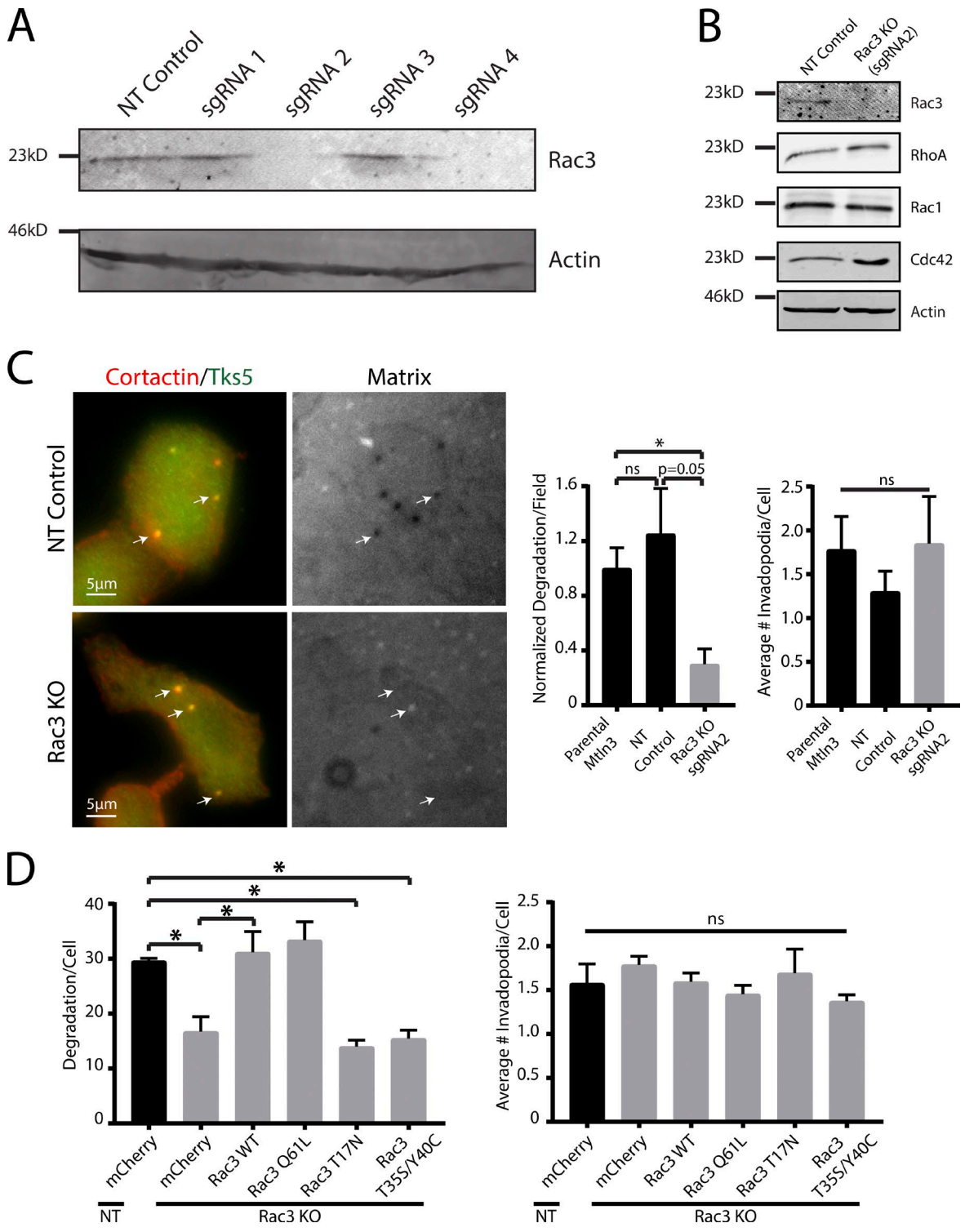

Figure S5. **CRISPR/Cas9 genetic editing of Rac3.** (A) Western blot of cell lysates from the CRISPR/Cas9 gene editing using the nontargeting (NT) control or four different guide RNAs targeting Rac3 in MTLn3 cells blotted for Rac3 and β-actin. (B) Western blot of cell lysates from NT control or sgRNA 2 Rac3-knockout (KO) MTLn3 cells blotted for Rac3, RhoA, Rac1, Cdc42, and β-actin. (C) Representative immunofluorescence images from nontargeting control (top) or Rac3 KO (bottom) MTLn3 cells plated on 405 nm fluorescent gelatin for 16 h. Invadopodia were visualized with cortactin and Tks5 antibodies. White arrows indicate invadopodia. (C, left graph) Normalized quantification of mean degradation area per field in parental, nontargeting control, or Rac3-knockout MTLn3 cells plated on 405 nm fluorescent gelatin for 16 h. $n \geq 10$ fields for each condition for each of three independent experiments. (C, right graph) Quantification of the mean number of invadopodia per cell for parental, nontargeting control, or Rac3-knockout MTLn3 cells. $n \geq 50$ invadopodia from ≥25 cells for each condition for three independent experiments. (D) Expression of Rac3 mutants in the CRISPR/Cas9 Rac3-knockout background. (D, left) Matrix degradation defect in Rac3-knockout is rescued only when WT or Q61L constitutively activated Rac3 was expressed. Expression of mCherry alone, T17N-DN Rac3, or T35S/Y40C effector binding (does not bind GIT1)–deficient mutant of Rac3 did not rescue the matrix degradation defect. (D, right) Mean number of steady-state invadopodia per cell was not impacted by either Rac3 knockout with mCherry expression alone or with the indicated mutants of Rac3 expressed over the Rac3-knockout background. *, $P \leq 0.05$. Error bars are SEM.

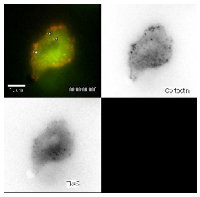

Video 1. **Invadopodia lifetimes in control cells.** Control MTLn3 cell transfected with two invadopodia markers, cortactin-mTagRFP and Tks5-EGFP, and time-lapse imaged every 2 min over 4 h. Cortactin and Tks5 fluorescence colocalization show invadopodia. Contrast is inverted, and arrowheads indicating invadopodia are added for clarity. Video is playing at seven frames per second. Widefield microscopy imaging was used.

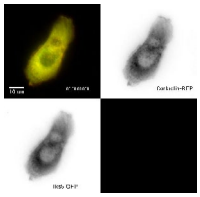

Video 2. **Invadopodia lifetimes are significantly reduced when Rac3 is depleted.** Rac3-depleted MTLn3 cell transfected with two invadopodia markers, cortactin-mTagRFP and Tks5-EGFP, and time-lapse imaged every 2 min over 4 h. Cortactin and Tks5 fluorescence colocalization show invadopodia. Contrast is inverted, and arrowheads indicating invadopodia are added for clarity. Video is playing at seven frames per second. Widefield microscopy imaging was used.

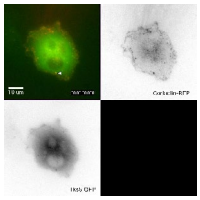

Video 3. **Invadopodia lifetimes are significantly reduced when CIB1 is depleted.** CIB1-depleted MTLn3 cell transfected with two invadopodia markers, cortactin-mTagRFP and Tks5-EGFP, and time-lapse imaged every 2 min over 4 h. Cortactin and Tks5 fluorescence colocalization show invadopodia. Contrast is inverted, and arrowheads indicating invadopodia are added for clarity. Video is playing at seven frames per second. Widefield microscopy imaging was used.

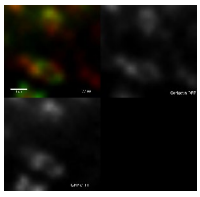

Video 4. **GIT1 oscillates between invadopodia core and the ring.** EGFP-GIT1 was expressed in MTLn3 cells, cotransfected with an invadopodia marker cortactin-mTagRFP, and imaged every minute for 1 h. Widefield microscopy imaging was used, followed by image deconvolution.

Reference

Smith, S.J., and K. Rittinger. 2002. Preparation of GTPases for structural and biophysical analysis. *Methods Mol. Biol.* 189:13–24.